Cell Metabolism
Resource

Complexome Profiling Identifies TMEM126B as a Component of the Mitochondrial Complex I Assembly Complex

Heinrich Heide,[1,6] Lea Bleier,[1,6] Mirco Steger,[1] Jörg Ackermann,[2] Stefan Dröse,[1] Bettina Schwamb,[3] Martin Zörnig,[3] Andreas S. Reichert,[4,5] Ina Koch,[2] Ilka Wittig,[1,*] and Ulrich Brandt[1,*]

[1]Molecular Bioenergetics Group, Medical School, Cluster of Excellence Frankfurt "Macromolecular Complexes," Goethe University, Theodor-Stern-Kai 7, 60590 Frankfurt am Main, Germany

[2]Molecular Bioinformatics Group, Institute of Computer Science, Faculty of Computer Science and Mathematics, Robert-Mayer-Straße 11–15, 60325 Frankfurt am Main, Germany

[3]Chemotherapeutisches Forschungsinstitut Georg-Speyer-Haus, Paul-Ehrlich-Straße 42–44, 60596 Frankfurt am Main, Germany

[4]Mitochondrial Biology, Buchmann Institute for Molecular Life Sciences, Goethe University Frankfurt am Main, Max-von-Laue-Straße 15, 60438 Frankfurt am Main, Germany

[5]Mitochondriale Biologie, Zentrum für Molekulare Medizin, Goethe Universität Frankfurt am Main, Max-von-Laue-Straße 15, 60438 Frankfurt am Main, Germany

[6]These authors contributed equally to this work

*Correspondence: wittig@zbc.kgu.de (I.W.), brandt@zbc.kgu.de (U.B.)

http://dx.doi.org/10.1016/j.cmet.2012.08.009

SUMMARY

Macromolecular complexes are essential players in numerous biological processes. They are often large, dynamic, and rather labile; approaches to study them are scarce. Covering masses up to ~30 MDa, we separated the native complexome of rat heart mitochondria by blue-native and large-pore blue-native gel electrophoresis to analyze its constituents by mass spectrometry. Similarities in migration patterns allowed hierarchical clustering into interaction profiles representing a comprehensive analysis of soluble and membrane-bound complexes of an entire organelle. The power of this bottom-up approach was validated with well-characterized mitochondrial multiprotein complexes. TMEM126B was found to comigrate with known assembly factors of mitochondrial complex I, namely CIA30, Ecsit, and Acad9. We propose terming this complex mitochondrial complex I assembly (MCIA) complex. Furthermore, we demonstrate that TMEM126B is required for assembly of complex I. In summary, complexome profiling is a powerful and unbiased technique allowing the identification of previously overlooked components of large multiprotein complexes.

INTRODUCTION

Macromolecular assemblies of proteins of different size and complexity play an essential role in a broad range of cellular processes. Such complexes may exist as stable entities or may form transient intermediates. Defining the composition and functional dynamics of such assemblies are formidable challenges, but the number of suitable methods is rather limited. Immunoprecipitation or tandem affinity protocols in combination with western blotting and mass spectrometry are widely used to identify interaction partners of specific proteins. However, these approaches are limited to a selected subset of the cellular interactome and provide hardly any insight into the actual composition and biochemical properties of the underlying complexes. To overcome these limitations, fractionation of the native complexes by mild nondestructive techniques like density gradient centrifugation, size-exclusion chromatography, and native electrophoresis is required. These approaches have been successfully applied to define even very large multiprotein complexes, e.g., the human centrosome (Andersen et al., 2003), pyruvate dehydrogenase and other complexes from chloroplasts (Olinares et al., 2010), and respiratory chain supercomplexes in mitochondria (Wittig et al., 2006b). Mass spectrometric analysis of samples fractionated by these techniques has been applied to identify the constituents of whole organelles (Foster et al., 2006) or multiprotein complexes (Wessels et al., 2009). Density gradient centrifugation requires rather large amounts of protein and suffers from low resolution. The use of better resolving size-exclusion columns leads to significant sample dilution and cannot be used for complexes larger than 5 MDa. Therefore, blue-native electrophoresis (BNE) (Wittig and Schägger, 2009; Wittig et al., 2006a) is the method of choice for sensitive and high-resolution fractionation of the "complexome" of entire cells or subcellular compartments. It has been demonstrated that even rather labile macromolecular assemblies can be separated by BNE and analyzed directly by mass spectrometry (Wessels et al., 2009; Sokolova et al., 2010; Remmerie et al., 2011). With the recently introduced large-pore blue-native electrophoresis (LP-BNE), now extremely large macromolecular assemblies up to a molecular mass of ~45 MDa can be separated (Strecker et al., 2010).

Here, we report the analysis of the entire complexome of intact rat heart mitochondria. Native complexes up to a size of ~30 MDa were separated by BNE and LP-BNE, and complexome profiles of the proteins identified by label-free quantitative

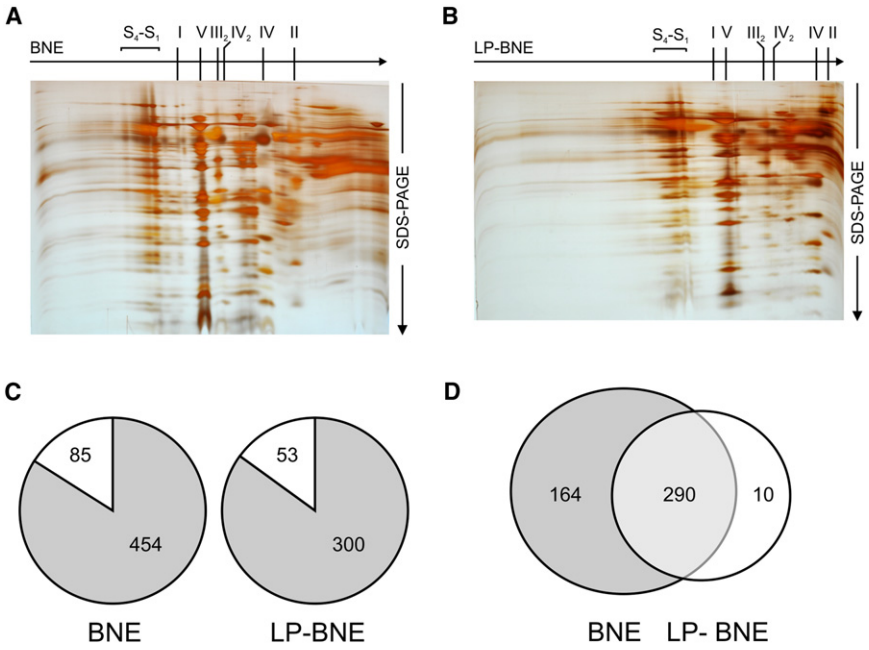

Figure 1. Separation of Mitochondrial Complexes by 2D BNE/SDS-PAGE and Assignment of Identified Proteins

S_4–S_1, respiratory supercomplexes as defined (Wittig et al., 2006b); I, II, IV, OXPHOS complexes I, II, IV; III_2, IV_2, dimers of OXPHOS complexes III, IV.

(A) First dimension 4%–16% acrylamide BNE gel, second dimension 16% SDS Tricine PAGE, followed by silver staining.

(B) First dimension 3%–9% acrylamide LP-BNE gel, second dimension 16% SDS Tricine PAGE, followed by silver staining.

(C) Proteins were assigned to mitochondria using the MitoMiner 2.0 tool (Smith and Robinson, 2009) and by the Mitoprot II algorithm (Claros and Vincens, 1996); probability score > 0.5. Grey, mitochondrial proteins; white, nonmitochondrial proteins.

(D) Venn diagram illustrating the fraction of mitochondrial proteins identified in both gel types.

mass spectrometry were constructed by hierarchical clustering. This bottom-up complexome profiling analysis allowed us to identify a number of soluble and membrane-bound macromolecular assemblies from different mitochondrial sub-compartments. We found TMEM126B as a previously overlooked component of the mitochondrial complex I assembly factor (MCIA) complex and show that this protein is indeed required for the formation of respiratory chain complex I.

RESULTS

Validation of the Complexome Profiling Approach

To establish and validate the complexome profiling approach, we used intact rat heart mitochondria as a readily available and defined subcellular compartment containing a number of well-characterized soluble and membrane bound multiprotein complexes. Mitochondria were prepared from hearts of young male Wistar rats. The respiration rate in the active state with glutamate/malate was 220 nmol O · mg^{-1} · min^{-1}, and the respiratory control factor was >9, indicating high purity and intactness of the mitochondria. After solubilization with the mild detergent digitonin, and separation by BNE and LP-BNE, second-dimension SDS-PAGE showed the typical and well established (Wittig et al., 2006a; Wittig et al., 2006b; Strecker et al., 2010) patterns of the complexes of the mitochondrial oxidative phosphorylation (OXPHOS) system, namely respiratory supercomplexes (S_4–S_1), and individual complexes (I–V) as monomers and dimers (Figures 1A and 1B). From the silver-stained gels, the presence of a number of additional complexes was evident that are difficult to define by this classical two-dimensional electrophoretic approach.

We cut native first dimension BNE and LP-BNE lanes into 60 even slices, subjected them to tryptic digest, and analyzed the resulting peptides by online nano-LC/ESI mass spectrometry. By matching spectra against the enhanced UniProt database for *Rattus norvegicus* (UniProt Consortium, 2012), we identified a total of 539 proteins in the BNE gel and 353 proteins in the LP-BNE gel. In both gel types, about 85% of the proteins could be assigned to mitochondria, confirming the high purity of the sample (Figure 1C). In total, 464 mitochondrial proteins were identified, of which 63% were present in both gels (Figure 1D).

Based on their relative abundance in different gel slices, the identified proteins were hierarchically clustered by uncentered correlation and single linkage with the Cluster 3.0 program (Eisen et al., 1998; de Hoon et al., 2004). From heat map illustrations of the resulting profiles (Figure 2 and Table S1, parts A and B, available online), groups of comigrating proteins are immediately apparent, of which the multiprotein complexes I–V of the OXPHOS system were most prominent. Reflecting their presence in supercomplexes of different composition, the subunits of complexes I, III, and IV were present in a number of different slices of the two gels. Also the previously reported formation of complex V monomers, dimers, and higher oligomers was clearly observed.

The respiratory chain complexes and their supercomplexes have been used previously to calibrate native gel systems (Strecker et al., 2010; Wittig et al., 2010; Ladig et al., 2011). A plot of the calculated molecular masses against the slices of the two gels, in which the respective complexes were identified by complexome profiling, shows that the migration distance of the complexes was proportional to the logarithm of their molecular masses (Figure S1). Based on this calibration, we estimated separation ranges up to ~7 MDa for the BNE gel and up to ~30 MDa for the LP-BNE gel, and we could assign approximate masses to the individual gel slices analyzed by LC-MS/MS (Table S1, parts A and B).

To validate our approach, we next determined which of the 90 constituent proteins of OXPHOS complexes I–V had been identified and how many of them were correctly grouped into the respective complexes (Table 1). In the BNE gel, 91% and in the LP-BNE gel, 86% of the known subunits were identified, of which almost 90% where correctly grouped into their respective

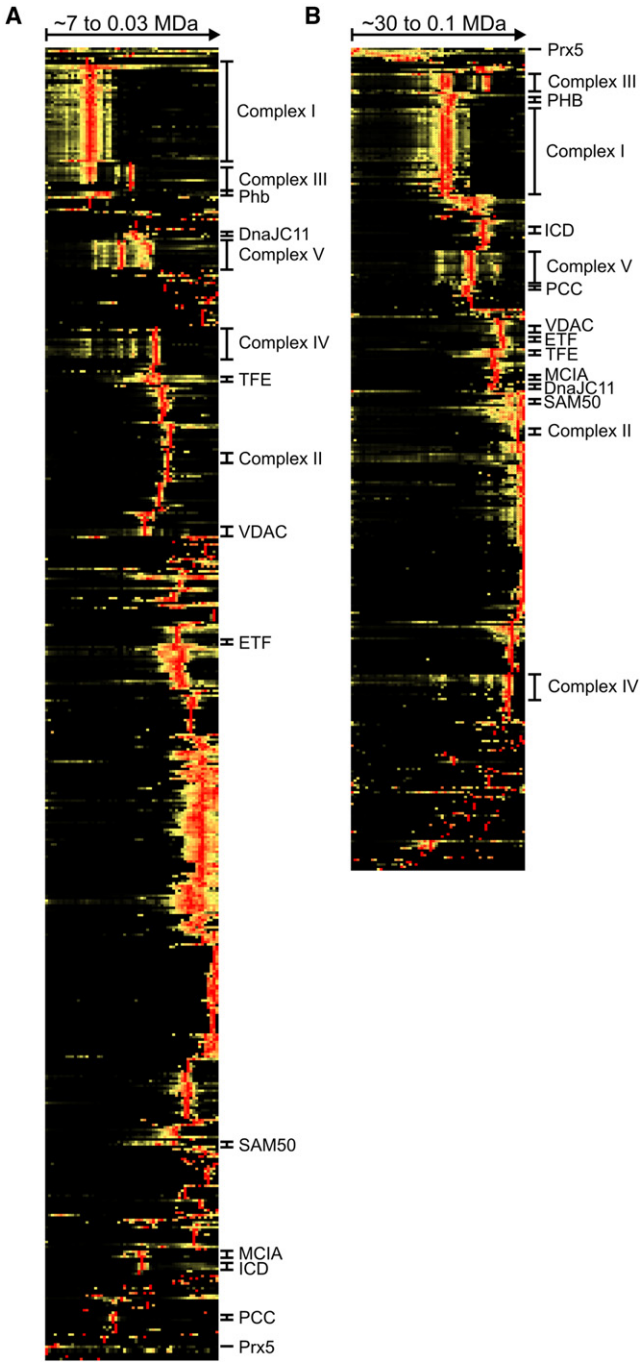

Figure 2. Overview Heat Maps of Complete Complexome Profiles
Positions of complexes are indicated. See Figure 3 for abbreviations and text for further details. For heat maps including details of the identified proteins, see Table S1, parts A and B. BNE (A) and LP-BNE (B) are shown. See also Figure S1 and Table S1.

complexes in both gels. The proteins not identified were either highly hydrophobic subunits (e.g., cytochrome *b* of complex III; subunits ND6 and ND4L of complex I) or were very small proteins of masses <10 kDa (Table S2). Both types of proteins tend to pose problems in a standard mass spectrometric analysis, since they give rise to only very few detectable peptides.

Table 1. Identification and Clustering Coverage of OXPHOS Complex Subunits

		LP-BNE		BNE	
Complex	Known Subunits[a]	Identified	Clustered	Identified	Clustered
I	45	40	37	42	38
II	4	4	3	4	4
III	11	9	7	10	9
IV	13	9	8	10	10
V	17	15	13	16	12
Total	90	77	68	82	73

See also Table S2.
[a]For a complete list of the identified subunits, see Table S1.

Mitochondrial Complexes Identified by Complexome Profiling

As evident from the heat map representations of the native gel profiles (Figure 2), a number of other proteins seemed to form large complexes. Based on their migration profile, they were grouped together by hierarchical clustering. To explore the potential of the complexome profiling approach, we analyzed a selected number of these complexes in more detail. The composition and characteristics of nine of these complexes are summarized in Table S3, and their migration patterns are shown in Figure 3.

The crystal structure of a 780 kDa $\alpha_6\beta_6$ dodecamer of propionyl-CoA carboxylase of the mitochondrial matrix (Figure 3A) has been solved recently (Huang et al., 2010). Indeed, this complex was found to migrate in both gel types at an apparent molecular mass that was very close to the calculated value. This indicated that the mass calibration (Figure S1) was also valid for soluble complexes. Mammalian NAD-dependent isocitrate dehydrogenase of the citric acid cycle is known to form an oligomeric complex with an $\alpha_2\beta_1\gamma_1$ subunit ratio of unknown multiplicity (Ramachandran and Colman, 1980). Well-defined apparent masses of 460 kDa in the LP-BNE and 300 kDa in BNE (Figure 3B) suggested that at least a $\alpha_6\beta_3\gamma_3$ multimer was present in rat heart mitochondria. This complex seemed to have lost one tetrameric unit under the conditions of BNE, which however was not observed as a separate entity. We conclude that in LP-BNE larger and more labile complexes could be retained, since also for the trifunctional enzyme, smaller complexes were detected in BNE (Figure 3C). For this enzyme complex of the fatty acid β-oxidation pathway, formation of an $\alpha_4\beta_4$ octamer has been reported (Uchida et al., 1992). However, this 508 kDa complex appeared as a minor component in both native gels. Rather, the $\alpha_2\beta_2$ tetramer seemed to be the dominant species, although a small amount of the even larger $\alpha_8\beta_8$ complex was also detectable at about 1,100 kDa. A 350 kDa complex in LP-BNE and a 170 kDa complex in BNE most likely corresponded to $\alpha_3\beta_2$ and $\alpha_1\beta_2$ breakdown products of larger species, as suggested by the relative intensities of the two proteins. In BNE, monomers were also observed. Electron transfer flavoprotein (ETF) shuttles reducing equivalents from the β-oxidation to the respiratory chain. In the LP-BNE profile, we observed complexes at apparent masses of about 250 kDa and 460 kDa that could correspond to the $\alpha_4\beta_4$ and $\alpha_8\beta_8$ heteromultimers of ETF (Figure 3D). In the BNE profile, the 60.5 kDa

heterodimer was detected, but the most prominent species was a 100 kDa complex that in addition contained the 42 kDa short chain acyl-CoA dehydrogenase, one of the physiological electron donors of ETF. The interaction between ETF and one of its electron donors, the medium chain specific acyl-CoA dehydrogenase, was modeled earlier in a molecular docking study (Roberts et al., 1996), but not observed experimentally. We also detected a whole series of different multimeric complexes of peroxiredoxin-5 ranging from 120 kDa to 24 MDa (Figure 3E). Peroxiredoxin-5 is a major component of the antioxidant defense in the mitochondrial matrix and belongs to the class of atypical 2-Cys peroxiredoxins (Cox et al., 2010). Redox state-dependent formation of dodecameric toroids and higher-ordered structures (filaments of laterally stacked toroids) has been observed for typical 2-Cys peroxiredoxins (Gourlay et al., 2003). In contrast, large multimeric structures, as observed here, have not been described before for atypical peroxiredoxins (Cox et al., 2010).

As the most prominent complex of the outer mitochondrial membrane, we observed a 270–280 kDa complex of the voltage dependent anion channel (VDAC) also known as mitochondrial porin. This mass came up as the dominant species in both gel types and fits well with the expected size of nonamers of all three isoforms (Figure 3F). Smaller oligomeric states of VDAC with variable stoichiometries have been reported before (Zalk et al., 2005; Gonçalves et al., 2007). As an example of a more complicated situation, we had a closer look at the complexes containing SAM50, a protein known to be involved in the assembly of mitochondrial outer membrane proteins, including VDAC (Kozjak-Pavlovic et al., 2007). Metaxin2 was proposed to be the mammalian analog of yeast SAM35, but its association with SAM50 has been challenged (Kozjak-Pavlovic et al., 2007). The two proteins exhibited a very similar migration profile and, suggesting a strong interaction, were grouped together by the clustering algorithm in both native gels (Figure 3G). Xie et al. (2007) suggested interactions of these two proteins with several other molecules including Metaxin1 and DnaJC11, which we also identified in both gels. Metaxin1 and DnaJC11 indeed were consistently found to group together and exhibited a profile that partially overlapped with that of SAM50 and Metaxin2. While the complexes migrating at around 250 kDa and 350 kDa seemed to contain all four proteins, the 190 kDa complex lacked DnaJC11, and the prominent peaks at around 120 kDa only contained SAM50 and Metaxin2 (Figure 3G, bottom panel). In the inner mitochondrial membrane, the prohibitins are known to form a ring-like chaperone complex of a total mass of 1.0–1.3 MDa (Nijtmans et al., 2000; Tatsuta et al., 2005). We found these multimeric structures in both profiles (Figure 3H). The LP-BNE profile showed almost exclusively the larger variant apparently containing 20 copies of each isoform of prohibitin, suggesting that this is the predominant native state of the complex.

TMEM126B Is Part of the Mitochondrial Complex I Assembly Complex

Another complex that could be assigned to the mitochondrial matrix had an apparent mass of 320 kDa and contained the two complex I assembly factors CIA30 (NDUFAF1) and Ecsit (Figure 3I). Functional interaction between CIA 30 and Ecsit and their presence in larger complexes has been reported, but these complexes have not been characterized in any detail (Vogel et al., 2007b). In addition to the 320 kDa complex that we observed in both gel types, a 540 kDa complex was found only in the BNE profile. In this case however, it seemed that, rather than from disintegration of the larger complex, this difference resulted from the fact that we simply failed to detect this species in LP-BNE. Even for the more abundant 320 kDa complex, the number of identified peptides and the sequence coverage was very low for both proteins in the LP-BNE profile (Table S1). Acad9, a recently identified complex I assembly factor reported to interact with CIA30 and Ecsit (Nouws et al., 2010), was also found to comigrate with these proteins, suggesting that it was also a component of this assembly factor complex. However, Acad9 was not grouped with the others by hierarchical clustering, because the migration profile differed due to a large fraction of monomer present in the mitochondria.

Interestingly, we found that TMEM126B, a mitochondrial transmembrane protein of so far unknown function also clustered with CIA30 and Ecsit by virtue of its highly similar BNE migration profile that it also shared with Acad9 (Figure 3I). To test whether TMEM126B was indeed a previously overlooked component of the complex I assembly machinery, we diminished *TMEM126B* expression in 143B osteosarcoma cells by lentiviral shRNA transduction. Quantitative real-time PCR revealed knockdown efficiencies of at least 60% for all six different shRNAs sequences (data not shown). A first assessment at the protein level by activity staining after high-resolution clear native electrophoresis (hrCNE) (Wittig et al., 2007) revealed markedly reduced amounts of complex I-containing supercomplexes with three of the short hairpin RNAs (shRNAs) (V2LHS_175840, V3LHS_365049, and V3LHS_365046; Figure S2A). In human mitochondria, complex I is found exclusively as a component of respiratory supercomplexes since it requires complex III for stability (Schägger et al., 2004; Moreno-Lastres et al., 2012). In all three knockdown cell lines transduced with *TMEM126B* shRNA and exhibiting strong effects on complex I assembly, the amount of *TMEM126B* mRNA was lowered by about 70% (Figure S2B).

For a more detailed analysis of the effects of *TMEM126B* knockdown on respiratory chain assembly and function we used the 143B cell line that had been lentivirally transduced by shRNA V2LHS_175840; hardly any supercomplex pattern could be observed in enriched mitochondrial membranes from these *TMEM126B* knockdown cells in silver-stained 2D BNE/Tricine SDS gels (Figure 4A). This finding was confirmed by BNE western blot (Figure 4B) and densitometric analysis. Compared to mock-transduced 143B cells, a residual level of only 5% complex I was present as component of respiratory supercomplexes in the *TMEM126B* knockdown cells (Figures 4B and 4C). In contrast, *TMEM126B* knockdown did not reduce the levels of respiratory complexes III, IV, and V. We noted that mock-transduced cells showed moderately higher levels of supercomplexes and individual complex IV compared to 143B parental cell line. The levels of complex III were significantly higher in *TMEM126B* knockdown cells (Figure 4C), which we attribute to the fact that less of the complex III dimer could be integrated in the respiratory supercomplexes.

To characterize the functional consequences of the *TMEM126B* knockdown, we first analyzed whole-cell respiration

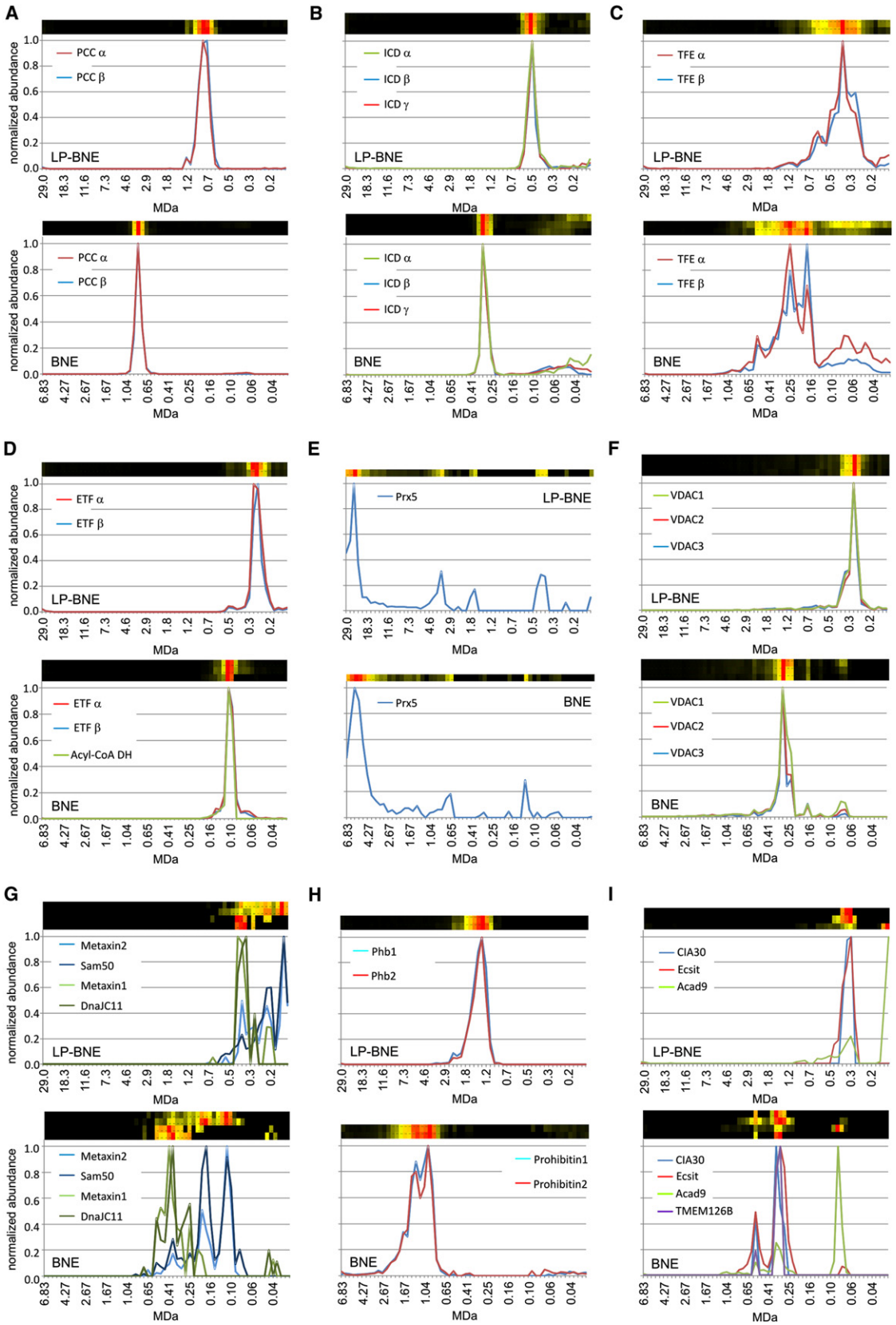
A
PCC α
PCC β
LP-BNE
BNE
normalized abundance
MDa
B
ICD α
ICD β
ICD γ
C
TFE α
TFE β
D
ETF α
ETF β
Acyl-CoA DH
E
Prx5
F
VDAC1
VDAC2
VDAC3
G
Metaxin2
Sam50
Metaxin1
DnaJC11
H
Phb1
Phb2
Prohibitin1
Prohibitin2
I
CIA30
Ecsit
Acad9
TMEM126B

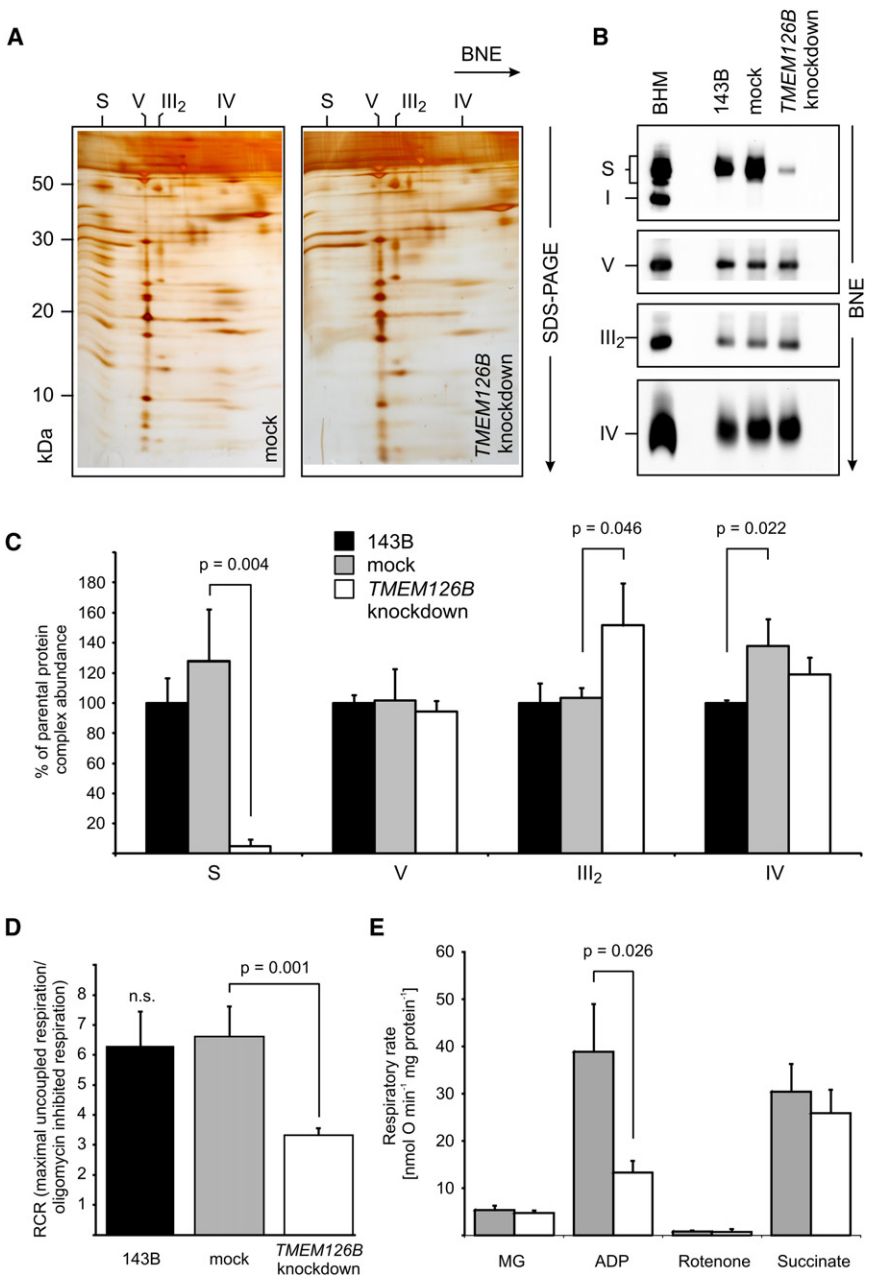

Figure 4. TMEM126B Knockdown Results in Complex I Defect

(A) Silver-stained 2D BNE/SDS tricine PAGE of enriched mitochondrial membranes.

(B) Representative BNE western blots of OXPHOS complexes in enriched mitochondrial membranes. CI-NDUFB8, CIII-Core2, and CV-α,β, were sequentially decorated on the same blot. CIV-COX6 was detected on a second blot.

(C) Densitometric quantification of OXPHOS complexes in BNE Western blots. Assignment of complexes: S, supercomplex containing complex I, III_2, and IV; III_2, complex III dimer; IV, complex IV; V, complex V/ATP synthase. BHM, bovine heart mitochondria as mass ladder.

(D) High-resolution respirometry of intact cells. The respiratory control ratio is expressed as ratio between maximally uncoupled respiration (after subsequent additions of 1 μM FCCP) and oligomycin (2 μg/ml) inhibited respiration.

(E) High-resolution respirometry of intact mitochondria from mock and *TMEM126B* knockdown cells. Substrates or inhibitors were added with the following concentrations: 4.8/5.6 mM malate/glutamate, 2 mM ADP, 10 μM rotenone, 5 mM succinate.

Data presented are the mean values of three independent experiments ± SD (C) or ± SEM (D and E). See also Figure S2.

by high-resolution respirometry. Consistent with the reduced levels of complex I, the respiratory control ratio as an indicator of tight coupling of oxidative phosphorylation and respiratory excess capacity was reduced by about 50% (Figure 4D). To further test whether the observed respiratory defect was indeed exclusively due to a complex I deficiency, we went on to isolate intact mitochondria from cultured cells by differential centrifugation. High-resolution respirometry revealed a reduction in respiration by about two-thirds after *TMEM126B* knockdown only when the electrons were fed into complex I via the NADH-linked substrates malate and glutamate in ADP-stimulated mitochondria (Figure 4E). In contrast, succinate driven respiration through complexes II, III, and IV was unaffected.

Next, we asked whether in the absence of TMEM126B the remaining complex I assembly factors were retained as a residual MCIA complex. Western blotting of 2D BNE/SDS-PAGE gels from intact mitochondria with anti-Acad9 and anti-CIA30 antibodies (Figure 5A) confirmed the presence of a 320 kDa MCIA complex in mock-transduced cells. In *TMEM126B* knockdown cells we observed a complex containing Acad9 and CIA30, but at a somewhat lower mass of 270 kDa. In contrast to mitochondria from rat heart (Figure 4I), in both samples complexes containing Acad9 and CIA30 were

Figure 3. Migration Profiles of Selected Complexes

Each panel shows the relative abundance of identified proteins plotted against the apparent molecular mass for LP-BNE (top) and BNE (bottom) gels. The colors used for each protein are indicated as a legend in the respective plot. Corresponding heat map segments are shown above each plot. See Table S3 and the main text for further details. propionyl-CoA carboxylase (PCC) complex (A), isocitrate-dehydrogenase (ICD) complex (NAD-dependent) (B), trifunctional enzyme (TFE) complex(C), electron-transferring flavoprotein (ETF) complex (D), peroxiredoxin-5 (Prx5) complex (E), voltage-dependent anion channel (VDAC) complex (F), SAM50/DnaJC11 complex, manually assembled (G) (see the main text for details), prohibitin complex (Phb) (H), and complex I assembly factor complex (I). Acad9 was added manually (see the main text). See also Figure S1 and Table S3.

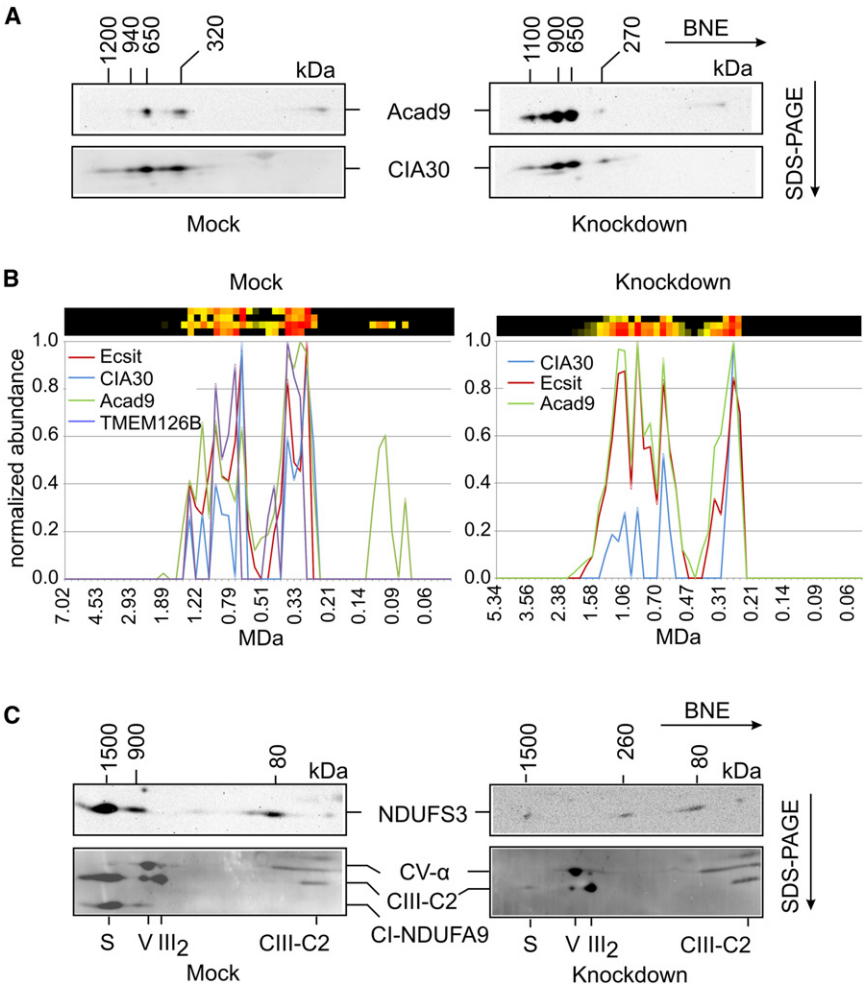

Figure 5. Effect of TMEM126B Knockdown on the Other Assembly Factors of the MCIA Complex

(A) 2D BNE/SDS-PAGE western blots of intact mitochondria isolated from mock and *TMEM126B* knockdown cells. Blots were decorated first with anti-Acad9 and subsequently with anti-CIA30 antibodies. Mass calibration was derived from the complexome profiling analysis performed in parallel.

(B) Migration profiles of the MCIA complex assembly factors obtained by complexome profiling of intact mitochondria isolated from mock-transduced and *TMEM126B* knockdown cells. The profiles are presented as indicated in the legend to Figure 3. OXPHOS complexes were used for mass calibration (data not shown).

(C) 2D BNE/SDS-PAGE western blots of enriched mitochondrial membranes of mock-transduced and *TMEM126B* knockdown cells, decorated first with anti-complex I-NDUFS3 (top panel) and afterward with an antibody mix detecting subunits of complex I and several OXPHOS complexes that were used for mass calibration. CV-α, α-subunit of complex V; CIII-C2, core 2 protein of complex III; CI-NDUFA9, subunit NDUFA9 of complex I; S, supercomplex S1; V, complex V; III_2, dimer of complex III.

detected also at higher masses above 600 kDa (Figure 5A). This was also evident when we analyzed the 143B cell lines by complexome profiling (Figure 5B). We reasoned that these larger complexes represented intermediates of complex I assembly that were present in detectable amounts only in the fast proliferating 143B cells, but not in the postmitotic heart muscle. We thus checked for the presence of two complex I subunits, NDUFS3 and NDUFA9, in these complexes by western blotting (Figure 5C). In mitochondrial membranes from mock-transduced cells, both subunits were detected mostly at about 1,500 kDa, representing their assembly into fully assembled complex I as part of a respiratory supercomplex S1. NDUFS3 seemed to be present also in a number of assembly intermediates with complexes at about 80 and 900 kDa being most prominent, while subunit NDUFA9 was only present in the 900 kDa band. In the *TMEM126B* knockdown cells only the early 80 kDa and 260 kDa assembly intermediates were detected by the NDUFS3 antibody. Consistent with the presence of a residual ~5% supercomplex (Figure 4), a weak signal at 1,500 kDa was also detected in the knockdown cells (Figure 5C). In the complexome profiles (Figure 5B), we further noted that the relative abundance of the larger complexes was different between the two cell lines, as was the relative distribution of CIA30. On the other hand, Acad9 was detected by mass spectrometry at lower masses only in the mock-transduced cells, although western blotting suggested that small amounts were also present in the knockdown cells (Figure 5A). These differences cannot be explained at present and will need further investigation.

For a more comprehensive assessment of the complex I assembly intermediates, we then analyzed the distribution of complex I subunits and complex I assembly factors in the complexome profiles of mock and knockdown cell lines (Figure 6). For comparison, we also included the subunits of complexes III and IV in this analysis. In the profile of mitochondria from mock cells, 40 of 45 subunits of complex I were identified in a complex of around 1,500 kDa. Confirming that this band corresponded to respiratory supercomplex S1, eight proteins of complex IV and 10 proteins of complex III were found to comigrate with these complex I subunits. Most of these proteins were also detected at about the same mass in mitochondria from *TMEM126B* knockdown cells, but as expected at much lower abundance. For complex IV, the monomer at about 220 kDa and for complex III, the dimer at about 470 kDa became the dominating species. Although the amount for many of the complex I subunits was too low for detection in the mass range below 1,200 kDa, the majority of them could be identified also here (Figure 6; note that for better visualization the normalization of the protein amounts were performed differently in the ranges above and below about 1,200 kDa). Like the proteins of the MCIA complex, the complex I subunits seemed to be distributed over a wide mass range reflecting a number of different assembly intermediates. Several

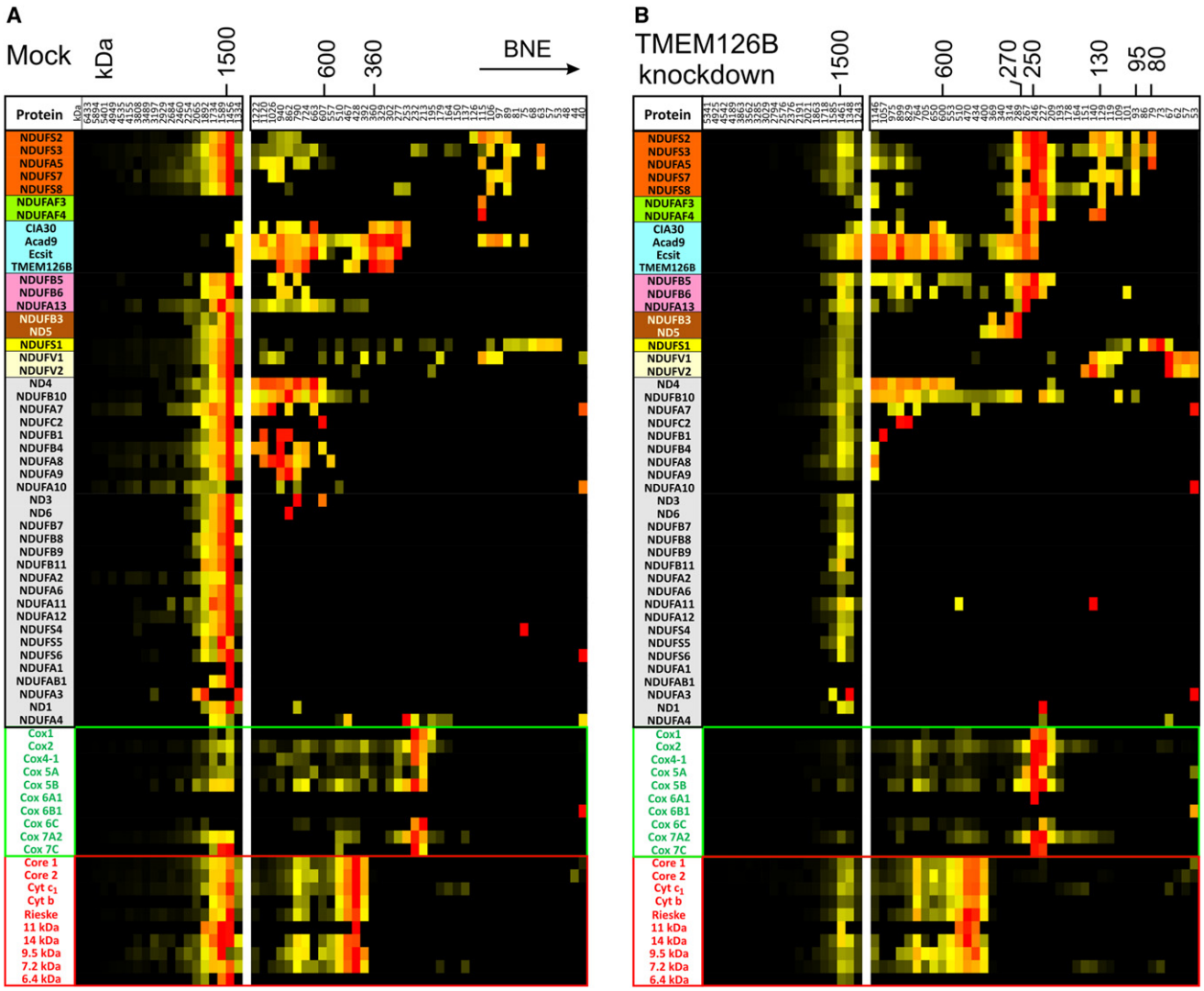

Figure 6. Respiratory Chain Complexes, Complex I Assembly Intermediates, and Assembly Factors in Mitochondria

Mock-transduced cells (A) and TMEM126B knockdown cells (B). Manually assembled partial complexome profiles of complex I subunits and assembly factors are shown as heat map representation. For the supercomplexes (left panels), the profiles from both cell lines were normalized together to enable direct quantitative comparison. For visualization of complex I assembly intermediates present in very small amounts, below 1,200 kDa the profiles were normalized separately, omitting the slices containing the supercomplexes (right panels). The colors used to group some of the identified proteins are explained in the main text.

important observations could be made that provided first insights into the function of the MCIA complex. In the mock-transduced cells, predominantly larger complex I assembly intermediates were found that were much less abundant in the *TMEM126B* knockdown cells. Several smaller intermediates of components of the Q module (Figure 6, orange) and the monomeric 75 kDa subunit NDUFS1 (Figure 6, yellow) were found in both cell lines. Interestingly, as expected from earlier studies (Vogel et al., 2007a), the assembly factors NDUFAF3 and NDUFAF4 (Figure 6, green) were found associated with the preformed Q module at about 120–130 kDa. These factors were also present in an ~250 kDa complex that prominently accumulated in the knockdown cells, suggesting that removal of TMEM126B had stalled assembly at this stage. In line with current models of complex I assembly (Mckenzie and Ryan, 2010), indications for the accumulation of other intermediates were also found, like an ~270 kDa complex containing NDUFB6 (Figure 6, pink) and a slightly larger complex containing subunit ND5 (Figure 6, brown). Moreover, the so-called flavoprotein, containing subunits NDUFV1 and NDUFV2, that is known to be integrated at a much later stage of assembly was found to accumulate in the knockdown cells (Figure 6, light yellow). Overall, these observations demonstrate that complexome profiling will also be a powerful tool to analyze the assembly process of multiprotein complexes. However, a more detailed analysis of complex I assembly would go far beyond the scope of the present study.

DISCUSSION

With the complexome profiling approach described here, it was possible to analyze the whole set of multiprotein assemblies in a subcellular compartment up to a molecular mass of ~30 MDa.

The proteomic profiles of the native gels yielded insight into the size, composition, and stability of soluble and membrane-bound complexes at very high resolution and sensitivity. The potential of the method could be clearly demonstrated, given that already the analysis of one sample with two different gel types under otherwise identical conditions provided a remarkable number of findings regarding the properties of different types of mitochondrial complexes. Not only prominent complexes like the components of the mitochondrial OXPHOS system, but also rather low abundant complexes, e.g., of the SAM50 system, were detected. Application of the hierarchical clustering approach that grouped proteins together based on their specific migration profile allowed us to differentially assign specific proteins even to complexes of similar or virtually identical size (Figure 4 and Table S3).

Some of the analyzed complexes behaved differently in the two gel types in the sense that they seemed to be less stable in BNE. In combination with information on the composition and size of the complexes also derived from the complexome profiles, these differences in stability can deliver valuable information on the network of protein-protein interactions. This is exemplified here by the differential association of SAM50 with the Metaxins and other proteins (Figure 4H). Thus, the use of two types of native gels, the standard BNE (Wittig et al., 2006a) and its large-pore variant LP-BNE (Strecker et al., 2010), not only extended the covered mass range, but also demonstrated another useful feature of the complexome profiling approach that opens a broad range of potential applications to study the dynamics and stability of macromolecular complexes. To this end, for specific applications in addition to the gel type and acrylamide gradient range, other experimental parameters like amount and type of the cathode buffer, detergents, pH value, and other additions used for solubilization can be varied to exploit the full potential of the method.

Using complexome profiling, we found TMEM126B—a mitochondrial protein of unknown function—associated with a complex I assembly factor complex (Figure 4I). Removal of this protein by shRNA-mediated gene knockdown in a human cell line almost completely and specifically abolished complex I assembly and severely impaired mitochondrial respiration, indicating that TMEM126B is indeed an essential component of the complex I assembly machinery. Ecsit and CIA30 have been shown to be associated with assembly intermediates of complex I and to be involved in the assembly of its membrane arm (Lazarou et al., 2007). Thus, it seems plausible that the crucial function of the membrane protein TMEM126B consists of recruiting the hydrophilic proteins CIA30, Ecsit, and Acad9 to the membrane to form a functional mitochondrial complex I assembly complex. An earlier study showed that knockdown of Ecsit resulted in decreased expression levels of CIA30 (Vogel et al., 2007b). In contrast, knockdown of *TMEM126B* had apparently no effect on the stability of the remaining soluble MCIA assembly factors, which were found to still form a complex in the absence of TMEM126B. Compared to the mock sample, the observed mass shift in the *TMEM126B* knockdown cells most probably resulted from loss of TMEM126B. In an earlier study, Vogel et al. had also observed large complexes at 850, 600, and 500 kDa containing the MCIA components Ecsit and CIA30 (Vogel et al., 2007b). Remarkably, predominantly larger assembly intermediates of complex I were also found in mock-transduced 143B cells but not in rat heart mitochondria. This may reflect a characteristic difference between fast-proliferating cells and a postmitotic tissue. Although we could not perform a more detailed analysis of the complex I assembly process within this study, overall our observations were in line with the current models of complex I assembly as reviewed recently (Mckenzie and Ryan, 2010).

The identification of TMEM126B as a subunit of the MCIA complex provides proof of principle that complexome profiling allows the discovery of functionally important components of macromolecular assemblies and assembly intermediates. Complexome profiling can be easily adapted to study other subcellular compartments than mitochondria or even the complexome of whole cells from various sources. Moreover, the dynamics and remodeling of macromolecular assemblies can now be studied in detail by comparing the profiles of biological samples, e.g., in gene knockout and knockdown studies or to study disease related changes in patients.

EXPERIMENTAL PROCEDURES

Cell Culture

HEK293T (human embryonic kidney) cells were cultured in DMEM (GIBCO Laboratories, Grand Island, NY) supplemented with 10% fetal bovine serum, 1% glutamine, and 1% penicillin/streptomycin in an atmosphere of 5% CO_2 at 37°C. 143B osteosarcoma cells (ATCC number CRL-8303) and 143B cells transduced either with lentiviral shRNAmir vector *pGIPZ* targeting *TMEM126B* (knockdown) or *pGIPZ* nonsilencing control shRNAmir (mock) were grown in tissue-culture flasks or roller bottles in DMEM culture medium (Sigma), 2 mM L-glutamine, 1 mM sodium pyruvate, 0.1 mg/ml uridine, nonessential amino acids, and 10% fetal bovine serum in a humidified cell incubator at 37°C under a 5% CO_2 atmosphere. For detachment, a Trypsin/EDTA solution (0.05%/0.02%) was used.

Generation of *TMEM126B* Knockdown Cell Lines

Viral particles of the human lentiviral *pGIPZ* shRNAmir *TMEM126B* set (RHS4531, Thermo Scientific) and nonsilencing *pGIPZ* lentiviral shRNAmir control (RHS4346) were produced in HEK293T cells. Cell transfection was carried out with 5.4 μl 10 mM polyethylenimine (PEI) per μg DNA. HEK293T cells (2×10^6) were transfected with 2.5 μg lentiviral shRNA construct together with 1.625 μg *p8.91* (Zufferey et al., 1997) and 0.875 μg *pMD2.G* packaging plasmids (Addgene, Cambridge, MA). Forty-eight and seventy-two hours after transfection, culture medium containing viral particles was supplemented with 8 μg/ml polybrene, added to 143B target cells for infection, and centrifuged for 60 min, 340 g, 32°C. 143B cells were transduced twice in 6-well plates at 1.5×10^5 cells per well. Successful knockdown of *TMEM126B* was confirmed by quantitative real-time PCR. Transduced 143B cells were selected in culture medium supplemented with 2 μg/ml puromycin.

Preparation of Mitochondria

Rat heart mitochondria were prepared as previously described (Dröse et al., 2006) from male Wistar rats (200–250 g) with all steps carried out at 4°C. Mitochondria were resuspended in 300 mM sucrose, 10 mM Na^+/HEPES (pH 7.4), 0.2 mM EDTA, and 1 mg/ml fatty-acid free bovine serum albumin. Intact mitochondria from cell culture were isolated by differential centrifugation. Cells were grown to confluence in tissue-culture roller bottles and harvested by trypsination and low-speed centrifugation (500 g, 10 min). All subsequent steps were carried out at 4°C. The cell pellet ($0.5–1.5 \times 10^8$ cells) was washed twice, first with 0.9% NaCl solution and then with mitochondria isolation medium (250 mM sucrose, 1 mM EDTA, and 20 mM Tris/HCl [pH 7.4]). Subsequently, cells were disrupted with a 10 ml syringe and a 20G cannula (ten strokes in total), followed by a low-speed centrifugation step (1,000 g, 10 min) to remove nuclei, cell debris, and intact cells. The mitochondria containing supernatant was transferred to a new tube and centrifuged with high speed (6,000 g, 10 min). The resulting mitochondria were resuspended in

mitochondria isolation medium. Protein quantification was performed via the Lowry method.

High-Resolution Respirometry

Mitochondrial respiration was analyzed at 25°C with an Oxygraph-2k system (OROBOROS Instruments, Innsbruck, Austria) and DatLab software. Rat heart mitochondria (0.3 mg protein) were added to 2 ml 250 mM sucrose, 10 mM Tris/HCl (pH 7.4), 10 mM potassium phosphate, and 10 μM EGTA. The respiratory control factor was determined as the ratio between active state after the addition of 2 mM ADP and controlled state with 4.8 mM malate/5.6 mM glutamate.

Mitochondria isolated from cultured cells (0.29–0.66 mg protein) were added to 2 ml solution containing 200 mM sucrose, 10 mM Tris/HCl (pH 7.4), 10 mM potassium phosphate, 10 mM magnesium sulfate, 2 mM EDTA, and NADH-linked substrates 4.8 mM malate/5.6 mM glutamate, feeding in electrons at complex I. The active state was induced by 2 mM ADP. Subsequently, complex II-dependent respiration was determined in the presence of the complex I inhibitor rotenone (10 μM) and 5 mM succinate. All respiratory rates were corrected for nonmitochondrial respiration by complete inhibition of the respiratory chain by 2 mM potassium cyanide.

Respiration of Trypsin-harvested cells suspended in 2 ml cultivation medium (~1.5 × 10^6/ml) was monitored at 37°C, and the respiratory control ratio was determined as the ratio between maximally uncoupled respiration (after subsequent additions of 1 μM FCCP) and oligomycin-inhibited (2 μg/ml) respiration.

Blue-Native Gel Electrophoresis

For complexome profiling, rat heart mitochondria were solubilized with digitonin at a detergent/protein ratio of 9 g/g in 50 mM NaCl, 2 mM 6-aminohexanoic acid, 1 mM EDTA, and 50 mM imidazole/HCl (pH 7.0). After centrifugation (22,000 g, 20 min 4°C), the solubilized mitochondrial proteins were applied to 0.5 × 0.15 cm gel wells (0.2 mg protein per lane) of a 4%–16% gradient BNE gel (Wittig et al., 2006a) and of a 3%–9% gradient LP-BNE gel (Strecker et al., 2010). Electrophoresis was started at 100 V and continued at 500 V after about 10 min. Duplicate 1D gel lanes were used for complexome profiling and second dimension 16% SDS Tricine gel electrophoresis (Schägger, 2006) followed by silver staining (Rais et al., 2004). Blue-native gel electrophoresis for complexome profiling of isolated mitochondria from transduced 143B cells was performed alike, but a digitonin to protein ratio of 6 g/g and a 3.5%–18% gradient BNE gel was used.

BNE for subsequent western blotting was performed with enriched mitochondrial membranes from cell homogenates or isolated mitochondria from cell culture. Cells were harvested in PBS and homogenized in 83 mM sucrose, 3.3 mM Tris/HCl (pH 7.5), 1.6 mM 6-aminohexanoic acid, and 0.3 mM EDTA. Nuclei and cell debris were removed by low-speed centrifugation for 5 min, at 500 g. Mitochondrial membranes were sedimented by centrifugation (10,000 g, 10 min, 4°C) and solubilized with digitonin (1 mg digitonin/10 mg cell wet weight) in 50 mM NaCl, 2 mM 6-aminohexanoic acid, 1 mM EDTA, and 50 mM imidazole/HCl (pH 7.0). After centrifugation (22,000 g, 20 min, 4°C), the protein content was measured, and 0.02 mg solubilized mitochondrial proteins were applied to 0.5 × 0.15 cm gel wells of a 4%–16% gradient BNE gel (Wittig et al., 2006a). Electrophoresis was started at 100 V and continued at 500 V after 10 min. BNE with intact mitochondria from cell culture was performed alike, but a digitonin to protein ratio of 6 g/g was used. 1D BNE gels were blotted or single lanes were loaded to SDS Tricine gels (16% acrylamide) for second-dimension electrophoresis followed by silver-staining or 2D western blotting (Schägger, 2006).

Western Blotting

1D BNE or 2D SDS gels were semidry electroblotted onto PVDF membranes as described (Wittig et al., 2006a; Schägger, 2006), and BNE-blots were destained in methanol. The blots were blocked in PBS containing 0.1% Tween and 1% bovine serum albumin. For immunodetection of OXPHOS complexes or MCIA components, the membranes were decorated with the following primary antibodies: anti-NDUFB8 (monoclonal, Invitrogen), anti-NDUFS3 (monoclonal, Mitosciences MS112), anti-OXPHOS (monoclonal, Mitosciences, MS603), anti-Acad9 (polyclonal, Sigma HPA037716), and anti-CIA30 (polyclonal, Sigma SAB1101401). Subsequently, the blots were incubated with the matching peroxidase-linked secondary antibodies (Sigma, against IgG from rabbits or mice). ECL Chemiluminescence was detected by a ChemiDoc XRS device (Biorad) and quantified with the Quantity One software package (Bio-Rad).

In-Gel Tryptic Digests

The in-gel digests were done in perforated well plates, essentially following the protocol by Collins et al. (2008). In brief, the 1D BNE or LP-BNE gel lanes were incubated in fixing solution (50% methanol, 10% acetic acid, 10 mM ammonium acetate [pH 3]) for 60 min. After two washes for 30 min with ultrapure water, the gel lanes were cut in 60 even 2 mm slices starting at the Coomassie dye front. Each gel slice was diced in smaller pieces before they were transferred into a well of a perforated 96-well plate (Proxeon, Denmark) containing 50 μl AHC buffer (50 mM ammonium hydrogen carbonate). Then, the slices were washed twice with 100 μl 50% methanol/AHC buffer for 30 min at room temperature under gentle agitation to remove excess Coomassie dye. After removal of the buffer by centrifugation, the gel pieces were incubated for 60 min with 50 μl 5 mM DTT in AHC, followed by the addition of 25 μl 30 mM iodoacetamide and incubation for another 45 min. For dehydration, 85 μl acetonitrile was added, and after 10 min, the solution was removed by centrifugation. The dehydrated gel pieces were swollen in 10 μl 5 ng/μl trypsin in 50 mM NH_4HCO_3, 10% acetonitrile, 1 mM $CaCl_2$ for 30 min at 4°C. Finally, the gel pieces were completely covered with AHC buffer, and the proteins were digested overnight at 37°C. The peptide-containing supernatants were collected by centrifugation into a fresh 96-well plate. The remaining peptides were extracted by 45 min incubation with elution solution (30% acetonitrile, 3% formic acid). After drying of the combined supernatants in a SpeedVac concentrator, the peptides were solubilized in 5% acetonitrile/0.5% formic acid for subsequent analysis by LC-MS.

Mass Spectrometry

Tryptic peptides were subjected to LC-MS/MS analysis in an Orbitrap XL mass spectrometer (Thermo) with an Agilent1200 nano-HPLC (high-performance liquid chromatography) at the front end. Peptides were separated on 3 μm C18 reversed phase silica beads filled into a 75 μm ID PicoTip emitter column (New Objectives) in 90 min HPLC runs using 60 min gradients of 5% to 50% acetonitrile with 0.1% formic acid, followed by a column wash with 90% acetonitrile and re-equilibration with 5% acetonitrile for 15 min each. Eluted peptides were analyzed in positive mode by a mass spectrometry method programmed to fragment the top ten most abundant precursor ions using dynamic exclusion for 3 min with a resolution of 30,000 at 400Th. Single-charged precursor ions were rejected, and doubly and higher charged ions were fragmented in the linear ion trap by CID at 35% collision energy. For accurate mass measurements, the lock mass option was enabled at m/z 445.120025 (Olsen et al., 2005). It is important to note that all 60 samples from one gel lane were subsequently analyzed under identical conditions without interruptions and with special attention to spray stability.

Protein Identification

The extraction of peak lists from RAW files and evaluation of spectra were performed with the Thermo Proteome Discoverer 1.2 environment with Mascot server 2.2 as the database search engine. The search parameters were set as follows: 8 ppm deviation on the precursor and 0.8 Da on fragment masses, fixed carbamidomethylation of cysteine, variable oxidation of methionine and trypsin as the protease (full tryptic with two missed cleavages allowed). Spectra were matched against the *Rattus norvegicus* reviewed protein database (7,628 sequences) obtained from UniProt (UniProt Consortium, 2012). The database was manually inspected for the presence of all known OXPHOS proteins and supplemented with additional 54 missing subunits identified by sequence alignment of the known sequences from *Mus musculus* using BLAST (Altschul et al., 1990). For advanced analysis, spectra were also matched against the unreviewed UniProt and NCBI database, which enabled identification of TMEM126B. Spectra obtained from mitochondria of human 143B osteosarcoma cells were matched against the UniProt *Homo sapiens* reviewed protein database. Spectra from the 60 gel slices of the complete gel lanes were batch-processed with Discoverer Daemon 1.2. The database search results were loaded as a multiconsensus report and filtered by the Mascot significance threshold filter set to 0.05. Keratins, hemoglobins and trypsin were removed from the list.

Label-Free LC/MS-Based Protein Quantification and Hierarchical Clustering

Peptide areas were extracted from the HPLC chromatograms with the precursor ions area detector node implemented into the Proteome Discoverer workflow with mass precision set to 3 ppm. For reconstruction of protein abundance profiles across the gel lane, the average areas of the three most abundant peptides per gel slice were exported from the Proteome Discoverer multiconsensus protein report to a MicrosoftExcel spreadsheet and used to construct protein abundance profiles. Peptides shared between similar proteins that were not unique were excluded with the Proteome Discoverer 1.2 proteins grouping option. The abundance distribution patterns of the identified proteins were evaluated for similarities and hierarchically grouped by distance measures based on Pearson correlation coefficient (uncentered) and single linkage clustering using Cluster 3.0 software (Eisen et al., 1998; de Hoon et al., 2004). Clustered profiles were visualized with Microsoft Excel.

Statistical Analysis

Results shown as mean ± SD or SEM. Differences were considered significant with a p value < 0.05 using an unpaired two-tailed Student's t test.

SUPPLEMENTAL INFORMATION

Supplemental Information includes Supplemental Experimental Procedures, two figures, and three tables and can be found with this article online at http://dx.doi.org/10.1016/j.cmet.2012.08.009.

ACKNOWLEDGMENTS

We are indebted to Hermann Schägger for many helpful suggestions and kindly providing antibodies. We thank Leo Nijtmans for helpful discussions. We are grateful for excellent technical assistance of Ilka Siebels, Gudrun Beyer, and Maximillian Mattil. Funding by the Deutsche Forschungsgemeinschaft (SFB815 Projects A2, Z1) and the BMBF (0315584A: GerontoMitoSys and 01GM1113B: mitoNET) is gratefully acknowledged. This study was supported by the Excellence Initiative of the German Federal and State Governments (EXC 115).

Received: January 2, 2012
Revised: May 9, 2012
Accepted: August 17, 2012
Published online: September 13, 2012

REFERENCES

Altschul, S.F., Gish, W., Miller, W., Myers, E.W., and Lipman, D.J. (1990). Basic local alignment search tool. J. Mol. Biol. *215*, 403–410.

Andersen, J.S., Wilkinson, C.J., Mayor, T., Mortensen, P., Nigg, E.A., and Mann, M. (2003). Proteomic characterization of the human centrosome by protein correlation profiling. Nature *426*, 570–574.

Claros, M.G., and Vincens, P. (1996). Computational method to predict mitochondrially imported proteins and their targeting sequences. Eur. J. Biochem. *241*, 779–786.

Collins, M.O., Yu, J.S., and Choudhary, J.S. (2008). Analysis protein complexes by 1D-SDS-PAGE and tandem mass spectrometry. Protocol Exchange. Published online June 18, 2008. http://dx.doi.org/10.1038/nprot.2008.123.

Cox, A.G., Winterbourn, C.C., and Hampton, M.B. (2010). Mitochondrial peroxiredoxin involvement in antioxidant defence and redox signalling. Biochem. J. *425*, 313–325.

de Hoon, M.J.L., Imoto, S., Nolan, J., and Miyano, S. (2004). Open source clustering software. Bioinformatics *20*, 1453–1454.

Dröse, S., Brandt, U., and Hanley, P.J. (2006). K+-independent actions of diazoxide question the role of inner membrane KATP channels in mitochondrial cytoprotective signaling. J. Biol. Chem. *281*, 23733–23739.

Eisen, M.B., Spellman, P.T., Brown, P.O., and Botstein, D. (1998). Cluster analysis and display of genome-wide expression patterns. Proc. Natl. Acad. Sci. USA *95*, 14863–14868.

Foster, L.J., de Hoog, C.L., Zhang, Y.L., Zhang, Y., Xie, X.H., Mootha, V.K., and Mann, M. (2006). A mammalian organelle map by protein correlation profiling. Cell *125*, 187–199.

Gonçalves, R.P., Buzhynskyy, N., Prima, V., Sturgis, J.N., and Scheuring, S. (2007). Supramolecular assembly of VDAC in native mitochondrial outer membranes. J. Mol. Biol. *369*, 413–418.

Gourlay, L.J., Bhella, D., Kelly, S.M., Price, N.C., and Lindsay, J.G. (2003). Structure-function analysis of recombinant substrate protein 22 kDa (SP-22). A mitochondrial 2-CYS peroxiredoxin organized as a decameric toroid. J. Biol. Chem. *278*, 32631–32637.

Huang, C.S., Sadre-Bazzaz, K., Shen, Y., Deng, B.B., Zhou, Z.H., and Tong, L.A. (2010). Crystal structure of the alpha(6)beta(6) holoenzyme of propionyl-coenzyme A carboxylase. Nature *466*, 1001–1005.

Kozjak-Pavlovic, V., Ross, K., Benlasfer, N., Kimmig, S., Karlas, A., and Rudel, T. (2007). Conserved roles of Sam50 and metaxins in VDAC biogenesis. EMBO Rep. *8*, 576–582.

Ladig, R., Sommer, M.S., Hahn, A., Leisegang, M.S., Papasotiriou, D.G., Ibrahim, M., Elkehal, R., Karas, M., Zickermann, V., Gutensohn, M., et al. (2011). A high-definition native polyacrylamide gel electrophoresis system for the analysis of membrane complexes. Plant J. *67*, 181–194.

Lazarou, M., McKenzie, M., Ohtake, A., Thorburn, D.R., and Ryan, M.T. (2007). Analysis of the assembly profiles for mitochondrial- and nuclear-DNA-encoded subunits into complex I. Mol. Cell. Biol. *27*, 4228–4237.

Mckenzie, M., and Ryan, M.T. (2010). Assembly factors of human mitochondrial complex I and their defects in disease. IUBMB Life *62*, 497–502.

Moreno-Lastres, D., Fontanesi, F., García-Consuegra, I., Martín, M.A., Arenas, J., Barrientos, A., and Ugalde, C. (2012). Mitochondrial complex I plays an essential role in human respirasome assembly. Cell Metab. *15*, 324–335.

Nijtmans, L.G.J., de Jong, L., Artal Sanz, M., Coates, P.J., Berden, J.A., Back, J.W., Muijsers, A.O., van der Spek, H., and Grivell, L.A. (2000). Prohibitins act as a membrane-bound chaperone for the stabilization of mitochondrial proteins. EMBO J. *19*, 2444–2451.

Nouws, J., Nijtmans, L., Houten, S.M., van den Brand, M., Huynen, M., Venselaar, H., Hoefs, S., Gloerich, J., Kronick, J., Hutchin, T., et al. (2010). Acyl-CoA dehydrogenase 9 is required for the biogenesis of oxidative phosphorylation complex I. Cell Metab. *12*, 283–294.

Olinares, P.D.B., Ponnala, L., and van Wijk, K.J. (2010). Megadalton complexes in the chloroplast stroma of Arabidopsis thaliana characterized by size exclusion chromatography, mass spectrometry, and hierarchical clustering. Mol. Cell. Proteomics *9*, 1594–1615.

Olsen, J.V., de Godoy, L.M.F., Li, G.Q., Macek, B., Mortensen, P., Pesch, R., Makarov, A., Lange, O., Horning, S., and Mann, M. (2005). Parts per million mass accuracy on an Orbitrap mass spectrometer via lock mass injection into a C-trap. Mol. Cell. Proteomics *4*, 2010–2021.

Rais, I., Karas, M., and Schägger, H. (2004). Two-dimensional electrophoresis for the isolation of integral membrane proteins and mass spectrometric identification. Proteomics *4*, 2567–2571.

Ramachandran, N., and Colman, R.F. (1980). Chemical characterization of distinct subunits of pig heart DPN-specific isocitrate dehydrogenase. J. Biol. Chem. *255*, 8859–8864.

Remmerie, N., De Vijlder, T., Valkenborg, D., Laukens, K., Smets, K., Vreeken, J., Mertens, I., Carpentier, S.C., Panis, B., De Jaeger, G., et al. (2011). Unraveling tobacco BY-2 protein complexes with BN PAGE/LC-MS/MS and clustering methods. J. Proteomics *74*, 1201–1217.

Roberts, D.L., Frerman, F.E., and Kim, J.J.P. (1996). Three-dimensional structure of human electron transfer flavoprotein to 2.1-A resolution. Proc. Natl. Acad. Sci. USA *93*, 14355–14360.

Schägger, H. (2006). Tricine-SDS-PAGE. Nat. Protoc. *1*, 16–22.

Schägger, H., de Coo, R., Bauer, M.F., Hofmann, S., Godinot, C., and Brandt, U. (2004). Significance of respirasomes for the assembly/stability of human respiratory chain complex I. J. Biol. Chem. *279*, 36349–36353.

Smith, A.C., and Robinson, A.J. (2009). MitoMiner, an integrated database for the storage and analysis of mitochondrial proteomics data. Mol. Cell. Proteomics *8*, 1324–1337.

Sokolova, L., Wittig, I., Barth, H.D., Schägger, H., Brutschy, B., and Brandt, U. (2010). Laser-induced liquid bead ion desorption-MS of protein complexes from blue-native gels, a sensitive top-down proteomic approach. Proteomics *10*, 1401–1407.

Strecker, V., Wumaier, Z., Wittig, I., and Schägger, H. (2010). Large pore gels to separate mega protein complexes larger than 10 MDa by blue native electrophoresis: isolation of putative respiratory strings or patches. Proteomics *10*, 3379–3387.

Tatsuta, T., Model, K., and Langer, T. (2005). Formation of membrane-bound ring complexes by prohibitins in mitochondria. Mol. Biol. Cell *16*, 248–259.

Uchida, Y., Izai, K., Orii, T., and Hashimoto, T. (1992). Novel fatty acid beta-oxidation enzymes in rat liver mitochondria. II. Purification and properties of enoyl-coenzyme A (CoA) hydratase/3-hydroxyacyl-CoA dehydrogenase/3-ketoacyl-CoA thiolase trifunctional protein. J. Biol. Chem. *267*, 1034–1041.

UniProt Consortium. (2012). Reorganizing the protein space at the Universal Protein Resource (UniProt). Nucleic Acids Res. *40* (Database issue), D71–D75.

Vogel, R.O., Dieteren, C.E.J., van den Heuvel, L.P.W.J., Willems, P.H.G.M., Smeitink, J.A.M., Koopman, W.J.H., and Nijtmans, L.G.J. (2007a). Identification of mitochondrial complex I assembly intermediates by tracing tagged NDUFS3 demonstrates the entry point of mitochondrial subunits. J. Biol. Chem. *282*, 7582–7590.

Vogel, R.O., Janssen, R.J., van den Brand, M.A.M., Dieteren, C.E.J., Verkaart, S., Koopman, W.J., Willems, P.H., Pluk, W., van den Heuvel, L.P., Smeitink, J.A., and Nijtmans, L.G. (2007b). Cytosolic signaling protein Ecsit also localizes to mitochondria where it interacts with chaperone NDUFAF1 and functions in complex I assembly. Genes Dev. *21*, 615–624.

Wessels, H.J.C.T., Vogel, R.O., van den Heuvel, L., Smeitink, J.A., Rodenburg, R.J., Nijtmans, L.G., and Farhoud, M.H. (2009). LC-MS/MS as an alternative for SDS-PAGE in blue native analysis of protein complexes. Proteomics *9*, 4221–4228.

Wittig, I., and Schägger, H. (2009). Native electrophoretic techniques to identify protein-protein interactions. Proteomics *9*, 5214–5223.

Wittig, I., Braun, H.P., and Schägger, H. (2006a). Blue native PAGE. Nat. Protoc. *1*, 418–428.

Wittig, I., Carrozzo, R., Santorelli, F.M., and Schägger, H. (2006b). Supercomplexes and subcomplexes of mitochondrial oxidative phosphorylation. Biochim. Biophys. Acta *1757*, 1066–1072.

Wittig, I., Karas, M., and Schägger, H. (2007). High resolution clear native electrophoresis for in-gel functional assays and fluorescence studies of membrane protein complexes. Mol. Cell. Proteomics *6*, 1215–1225.

Wittig, I., Beckhaus, T., Wumaier, Z., Karas, M., and Schägger, H. (2010). Mass estimation of native proteins by blue native electrophoresis: principles and practical hints. Mol. Cell. Proteomics *9*, 2149–2161.

Xie, J., Marusich, M.F., Souda, P., Whitelegge, J., and Capaldi, R.A. (2007). The mitochondrial inner membrane protein mitofilin exists as a complex with SAM50, metaxins 1 and 2, coiled-coil-helix coiled-coil-helix domain-containing protein 3 and 6 and DnaJC11. FEBS Lett. *581*, 3545–3549.

Zalk, R., Israelson, A., Garty, E.S., Azoulay-Zohar, H., and Shoshan-Barmatz, V. (2005). Oligomeric states of the voltage-dependent anion channel and cytochrome c release from mitochondria. Biochem. J. *386*, 73–83.

Zufferey, R., Nagy, D., Mandel, R.J., Naldini, L., and Trono, D. (1997). Multiply attenuated lentiviral vector achieves efficient gene delivery in vivo. Nat. Biotechnol. *15*, 871–875.